ChemComm

ROYAL SOCIETY OF CHEMISTRY

COMMUNICATION

View Article Online
View Journal | View Issue

Cite this: *Chem. Commun.*, 2020, **56**, 301

Received 2nd October 2019,
Accepted 20th November 2019

DOI: 10.1039/c9cc07750b

rsc.li/chemcomm

A self-assembling amphiphilic dendrimer nanotracer for SPECT imaging†

Ling Ding,[ab] Zhenbin Lyu,[a] Aura Tintaru,[c] Erik Laurini,[d] Domenico Marson,[d] Beatrice Louis,[ef] Ahlem Bouhlel,[ef] Laure Balasse,[ef] Samantha Fernandez,[ef] Philippe Garrigue,[ef] Eric Mas,[g] Suzanne Giorgio,[a] Sabrina Pricl,[dh] Benjamin Guillet[ef] and Ling Peng *[a]

Bioimaging has revolutionized modern medicine, and nanotechnology can offer further specific and sensitive imaging. We report here an amphiphilic dendrimer able to self-assemble into supramolecular nanomicelles for effective tumor detection using SPECT radioimaging. This highlights the promising potential of supramolecular dendrimer platforms for biomedical imaging.

Medical imaging plays an important role in modern medicine by providing accurate information relating to diagnosing, grading and staging diseases as well as monitoring treatment response and efficacy.[1] Among the commonly used non-invasive imaging modalities such as magnetic resonance imaging (MRI), computed tomography (CT), positron emission tomography (PET), single photon emission computed tomography (SPECT), and ultrasonography (US), PET and SPECT have the highest sensitivity, and are able to visualize functional information quantitatively, which is very important for disease assessment and diagnosis and personalized medicine.[1–5] Nanotechnology can further enhance the sensitivity and specificity of molecular imaging *via* the "Enhanced Permeation and Retention (EPR)" effect (also named passive tumor targeting).[6–8] EPR results in nanoparticle specific tumor accumulation thanks to the leaky vasculature and dysfunctional lymphatic system characterizing the tumor microenvironment.[9] In addition, nanosystems carrying and incorporating abundant imaging reporters can significantly amplify the contrast signal for better imaging and diagnosis. Consequently, a myriad of nanosystems have been explored for PET and SPECT imaging of tumors.[2,6,10]

We have recently used the self-assembling amphiphilic dendrimer **Ga-1** to establish an innovative nanotracer for PET imaging (Fig. 1).[11] This dendrimer is composed of a long hydrophobic alkyl chain and a hydrophilic poly(amidoamine) (PAMAM) dendron bearing the PET radionuclide ^{68}Ga(III) complexed within the macrocyclic chelator NOTA (1,4,7-triazacyclononane-1,4,7-triacetic acid) at the peripheral units (**Ga-1** in Fig. 1). It self-assembles into small and stable nanomicelles, which can effectively accumulate in tumors. These nanomicelles deliver excellent results in PET imaging of different tumors, including some which could not be detected with the standard clinical PET agent [^{18}F]FDG (2-fluorodeoxyglucose).[11] The performance of this dendrimer radiotracer is largely ascribed to the beneficial combination of its unique multivalent dendrimeric structure and the relevant EPR effect.

Motivated by the promising PET imaging results,[11] we aimed at further exploiting self-assembling nanotechnology for constructing

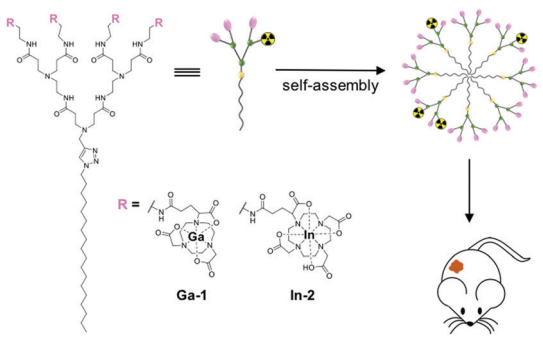

Fig. 1 Self-assembling dendrimer nanosystems based on the amphiphilic dendrimers **1** and **2** bearing radionuclide, for positron emission tomography (PET) and single photon emission computed tomography (SPECT) imaging of tumors, respectively.

[a] *Aix Marseille Univ, CNRS, Centre Interdisciplinaire de Nanoscience de Marseille (UMR 7325), Equipe Labellisée Ligue Contre le Cancer, Marseille, France. E-mail: ling.peng@univ-amu.fr*
[b] *Aix Marseille Univ, CNRS, CRMBM, Marseille, France*
[c] *Aix Marseille Univ, CNRS, Institut de Chimie Radicalaire (UMR7273), Marseille, France*
[d] *Molecular Biology and Nanotechnology Laboratory (MolBNL@UniTS), DEA, University of Trieste, Trieste, Italy*
[e] *Aix Marseille Univ, INSERM, INRA, C2VN, Marseille, France*
[f] *Aix Marseille Univ, CNRS, Centre Européen de Recherche en Imagerie Médicale (CERIMED), Marseille, France*
[g] *Aix Marseille Univ, CNRS, INSERM, Institut Paoli-Calmettes, Centre de Recherche en Cancérologie de Marseille (CRCM), Marseille, France*
[h] *Department of General Biophysics, Faculty of Biology and Environmental Protection, University of Lodz, Lodz, Poland*

† Electronic supplementary information (ESI) available. See DOI: 10.1039/c9cc07750b

effective dendrimer-based radiotracers for SPECT imaging. Different from PET, SPECT has the capacity to image multiple processes simultaneously by using the corresponding detection windows of different radionuclides with distinct gamma ray energies.[1–3] In addition, SPECT is more readily accessible and less expensive than PET in the clinics, even if PET has higher sensitivity and resolution. Recent progress in advanced detection technology and the combination with computed tomography (CT) has considerably improved the resolution and sensitivity of SPECT, placing SPECT as a quantitative imaging modality similar to PET.[3,12] Also, SPECT radiotracers generally have longer half-lives, which allows the characterization of slow kinetic processes and long biological events that take hours or days. Common radionuclides used in SPECT imaging include technetium-99m ([^{99m}Tc]Tc), indium-111 ([^{111}In]In) and iodine-123 ([^{123}I]I). Although [^{99m}Tc]Tc is the most widely used, [^{111}In]In has a relatively longer half-life (2.8 days). Accordingly, in this study, we chose [^{111}In]In as the radionuclide to develop a dendrimer radiotracer for SPECT imaging with the aim of monitoring and measuring long and slow biological processes such as tumor development and treatment.

Chelation of $^{111}In^{3+}$ to a thermodynamically stable and kinetically inert complex is a fundamental requirement for SPECT imaging in order to prevent the release of free radionuclide.[4,5] The cyclic chelator DOTA (1,4,7,10-tetraaza-cyclododecane-1,4,7,10-tetraacetic acid) and the acyclic chelator DTPA (diethylenetriaminepentaacetic acid) are the most frequently used in nuclear medicine.[13] In general, DOTA forms more stable complexes with radionuclide ions than the acyclic chelator DTPA because of the entropically favorable pre-organized and rigid binding sites within the DOTA ring. Nevertheless, the process of metal-complex formation is often slow for DOTA, and requires high temperature and long reaction times. Yet, as DOTA is the "gold standard" chelator for $^{111}In^{3+}$,[13] and on the basis of our previous experience in developing the NOTA-conjugated dendrimer to complex with the radionuclide Ga^{3+} (**Ga-1**) for PET imaging (Fig. 1),[11] we selected DOTA as the chelator to construct the amphiphilic dendrimer **2** which, in turn, was complexed with $^{111}In^{3+}$ to generate **In-2** for SPECT imaging (Fig. 1 and 2). Knowing that the DOTA ring is considerably larger than that of NOTA, we initially worried about the eventual synthetic difficulty stemming from steric hindrance of the DOTA terminals in **2**. Gratifyingly, we could reliably synthesize the DOTA-conjugated dendrimer **2** with high yield (Fig. 2A). Also of note, we successfully prepared the stable dendrimer complex **In-2** at 37 °C within 2 hours. Importantly, **In-2** self-assembled into small and uniform nanomicelles for effective SPECT imaging of tumors. We present below the synthesis and characterization of the amphiphilic dendrimer **2** and its complex with In^{3+} as well as the nanomicelles formed with the obtained dendrimer **In-2** for SPECT imaging.

Similar to our previous synthesis of the NOTA-dendrimer **1**,[11] we conjugated the amine-terminated amphiphilic dendrimer with the reagent DOTA-GA(tBu)$_4$, followed by deprotection for preparing **2** (Fig. 2A). Compared to the synthesis of **1**, we halved the quantity of the reagent DOTA-GA(tBu)$_4$ from 4 to 2 equivalents, which considerably simplified the purification procedure while maintaining the high synthesis yield of 88% for **2**. The chemical structure and integrity of **2** was analyzed and confirmed using ^{1}H, ^{13}C and 2D NMR and high-resolution mass spectrometry (HRMS), which exhibited the signals characteristic of the chemically conjugated DOTA groups (Fig. S1 and S2, ESI†). Chelation of the stable isotope $^{115}In^{3+}$ by **2** was performed using $^{115}InCl_3$ at 37 °C, pH 5.0 for 2 hours (Fig. 2A), and the final dendrimer **In-2** was obtained in pure form as a white solid after dialysis to remove the free $^{115}In^{3+}$. The successful complexation of four $^{115}In^{3+}$ by each molecule of the dendrimer **2** was confirmed using HRMS, which showed the isotopic pattern characteristic of the triply charged species [^{115}**In-2** + 3H]$^{3+}$ in addition to the expected molecular weight peak (Fig. 2B and Fig. S3B, ESI†).[14] It is important to mention that the formation of DOTA complexes with metal ions usually requires high temperature at 95 °C and long reaction time of several hours because of the slow binding kinetics of DOTA. Remarkably, we successfully chelated In^{3+} with the DOTA-conjugated dendrimer **2** at relatively low temperature (37 °C) within 2 h. This may be ascribed to the steric congestion created at the dendrimer terminals,[15] making the DOTA entities in **2** more reactive and hence favorably promoting their complexation with In^{3+} rapidly and at lower temperature to form the stable complex **In-2**.

To corroborate the reliable synthesis of **In-2**, we studied the formation of the complex between dendrimer **2** and In^{3+} using isothermal titration calorimetry (ITC). Specifically, a solution of **2** at 100 μM was titrated with the solution of $InCl_3$ at pH = 5.0 and 37 °C (see the ESI† for details). The left panel in Fig. 2C shows that the interaction between the DOTA cages of **2** and the In^{3+} cations is characterized by a robust exothermic behavior, reflecting an enthalpy-driven binding process (ΔH = −5.25 kcal mol^{-1}) led by strong coordination interactions between the In^{3+} and the DOTA cages of **2**. Notably, the entropic component ($-T\Delta S$ = −2.61 kcal mol^{-1}) also favors the stability of **In-2**. This is probably due to a synergistic effect of the hydrophobic interactions between the apolar dendrimer tails, which aggregate together with the concomitant release of water and ions from the charged surfaces when they form complexes with the cations. Accordingly, the spontaneous formation of the **In-2** complex is highly thermodynamically favorable, with a Gibbs free energy (ΔG) value of −7.86 kcal mol^{-1}. Interestingly, ITC measurements show that the number of $^{115}In^{3+}$ in **In-2** is 4.02, which confirms the ideal stoichiometry of 4 : 1. Taken together, the ITC results provide evidence that the synthesis of **In-2** was successful, and that **In-2** is a stable complex.

We next studied the self-assembly of **In-2** in solution. **In-2** spontaneously self-assembled into small and spherical nanoparticles with average dimensions around 18 nm, as revealed by transmission electron microscopy (TEM) (Fig. 3A). Also, dynamic light scattering (DLS) analysis confirmed the formation of small nanoparticles with sizes around 19 nm, which is typical for nanomicelles (Fig. 3B). The formed nanoparticles were stable, with the critical micelle concentration (CMC) being 60 ± 10 μM (Fig. S4, ESI†). Further molecular dynamics (MD) simulations confirmed the spontaneous aggregation of **In-2** into spherical micelles. Fig. 3C illustrates a representative configuration of the

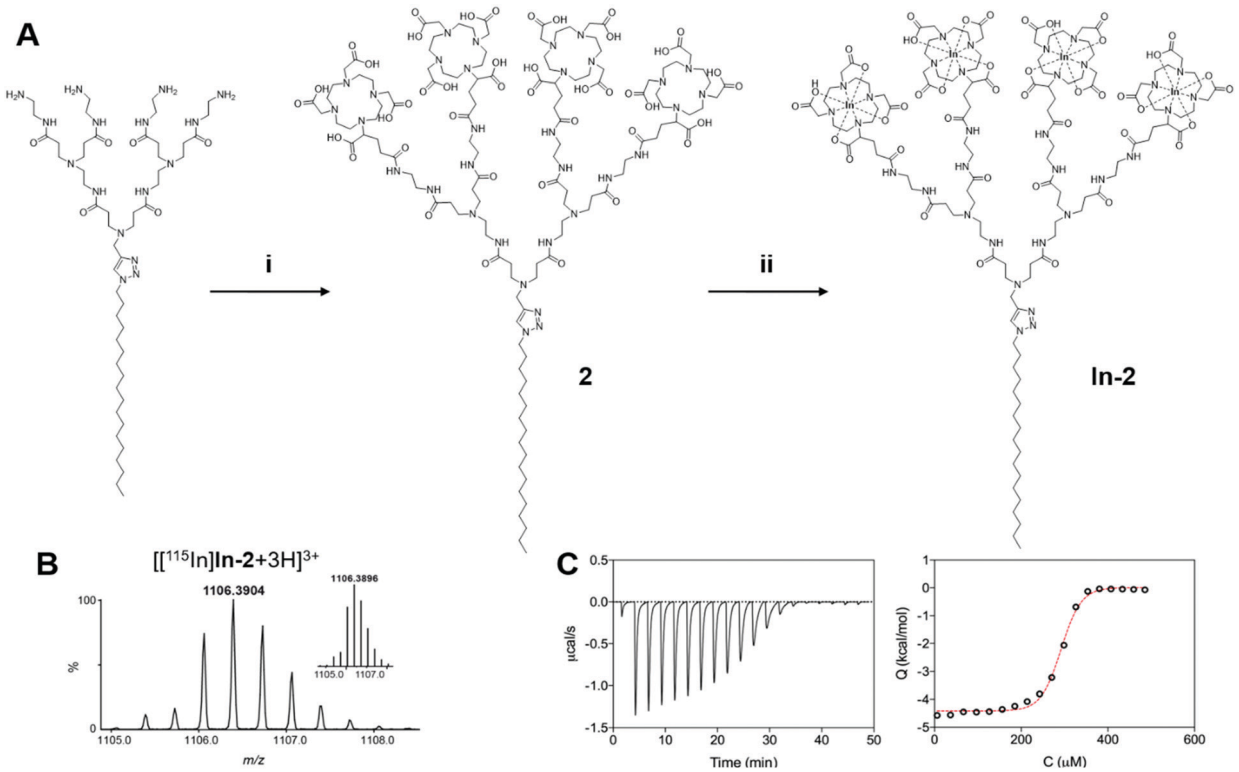

Fig. 2 Synthesis of the amphiphilic dendrimer **2** bearing DOTA units and its chelation with the nonradioactive isotope $[^{115}In]In^{3+}$ at the terminals to deliver the dendrimer **In-2**. (A) Synthesis scheme: (i) (a) DOTA-GA(*t*Bu)$_4$, PyBOP, NMM, DMF, 30 °C, 72 h; (b) TFA, CH_2Cl_2, 30 °C, 24 h. (ii) $[^{115}In]InCl_3$, 1.0 M HCl, 37 °C, 2 h. (B) High-resolution mass spectrum (HRMS) showing the isotopic pattern of the observed triply charged species $[[^{115}In]$**In-2** + 3H$]^{3+}$. The inset shows the calculated isotopic pattern. (C) Isothermal titration calorimetry (ITC) curve (right) for chelation of In^{3+} with the dendrimer **2**. The left panel shows measured heat power *versus* time elapsed during titration.

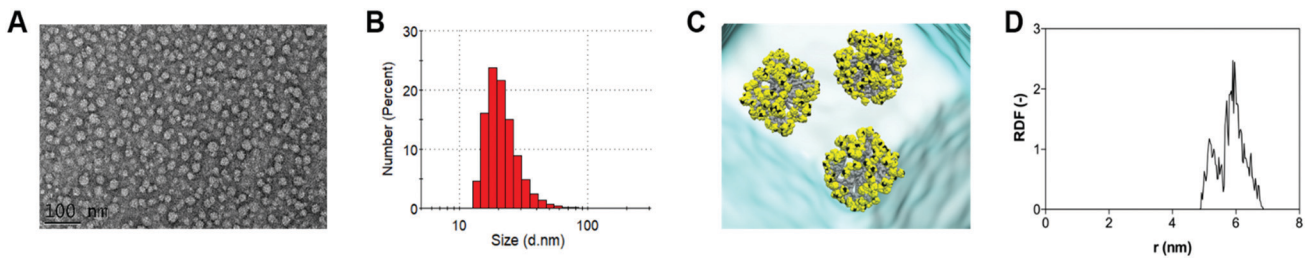

Fig. 3 Self-assembling of the amphiphilic dendrimer **In-2** into small and uniform nanomicelles. (A) Transmission electron microscopy (TEM) image, (B) dynamic light scattering (DLS) measurement, and (C and D) computer modeling of the self-assembled nanoparticles formed by **In-2**. (C) Final image of the **In-2** self-assembly process into spherical micelles as obtained from atomistic molecular dynamics (MD) simulations. The different parts of the **In-2** molecules are represented as spheres (atom color: grey, hydrocarbon chain; yellow, DOTA cage; black, In^{3+}), while water molecules are shown as aqua transparent spheres. The first water shell surrounding each molecule/micelle is highlighted as a light cyan transparent contour. (D) Radial distribution function of the In(III)-bearing terminals as a function of the distance from the center of mass of the **In-2** micelles.

stable **In-2** micelles obtained at the end of the computational process starting from a random distribution of **In-2** in solution. The calculated average micelle diameter was around 15 nm, in close agreement with the values obtained using experimental techniques (TEM and DLS). Along the entire MD trajectories, all the In^{3+}/DOTA terminal groups were nicely located at the micellar periphery without any back-folding observed, as evident from the relevant radial distribution function of the terminal groups shown in Fig. 3D.

Encouraged by the favorable self-assembly properties of **In-2**, we prepared the corresponding radioactive dendrimer complex $[^{111}In]$**In-2** for SPECT imaging. We obtained the $[^{111}In]$**In-2** complex with a satisfying radiochemical purity over 91 ± 2% along with a high molar activity of 1.09 ± 0.15 GBq µmol^{-1}. In addition, this radiochemical purity and integrity was maintained for up to 30 hours at 37 °C in human serum (Fig. 4A). On the basis of the high radiochemical purity and stability, we performed SPECT imaging using $[^{111}In]$**In-2** in orthotopically xenografted mice bearing tumors derived from a human pancreatic adenocarcinoma tumor cell line, SOJ-6 (Fig. 4B). Co-registration with CT enabled precise, anatomical localization of SPECT signals for further quantification. The biodistribution of

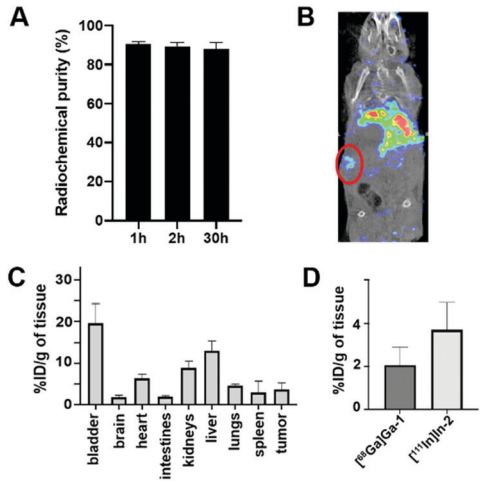

Fig. 4 Radiolabeled dendrimer [^{111}In]**In-2** for SPECT imaging in a mouse orthotopic xenograft model of pancreatic adenocarcinoma (SOJ-6 cell line). (A) [^{111}In]**In-2** radiochemical purity and stability in human serum at 37 °C for at least 30 h was assessed by radio-thin layer chromatography. (B) Representative μSPECT/CT image of [^{111}In]**In-2** 180 minutes after intravenous injection. Orthotopic SOJ6 tumor is highlighted by the red circle (n = 3 mice). (C) Biodistribution of [^{111}In]**In-2** quantified in each organ by μSPECT/CT 180 min after injection. Results are expressed as the mean percentage of injected dose per gram of tissue (n = 3 mice). (D) Tumor uptake comparison between [^{68}Ga]**Ga-1** and [^{111}In]**In-2** in the same mice (n = 3).

[^{111}In]**In-2** mapped by SPECT has obvious similarities with that obtained with [^{68}Ga]**Ga-1** using PET (Fig. 4B and Fig. S4, ESI†).[11] [^{111}In]**In-2** showed hepatic retention and elimination through the urinary tract (Fig. 4C and Fig. S4B, ESI†), similar to what was observed for [^{68}Ga]**Ga-1** using PET,[11] and many other nanoparticles.[2,6–8] Notably, the hepatic uptake of [^{111}In]**In-2** was 2-fold higher than we previously observed for [^{68}Ga]**Ga-1**, along with a higher kidney retention (Fig. S4B, ESI†). The tumor uptake of [^{111}In]**In-2** was almost 2-fold higher than that of [^{68}Ga]**Ga-1** (Fig. 4D and Fig. S4, ESI†), and the duration of the signal was also more stable and longer. This difference may stem from the different chelators, and the resulting negatively charged [^{111}In]-**In-2** and neutral [^{68}Ga]**Ga-1**, as well as the slightly different size of [^{111}In]**In-2** and neutral [^{68}Ga]**Ga-1**. In addition, [^{111}In]In has a longer half-life than [^{68}Ga]Ga. Altogether, these results confirm the high flexibility and modularity of our dendrimer nanosystems for bioimaging.

In conclusion, we have developed a supramolecular dendrimer nanosystem based on self-assembly of the amphiphilic dendrimer **In-2** for SPECT imaging in an orthotopic tumor-xenograft mouse model. The work present here alongside our previous studies on PET imaging[11] and drug delivery,[16–18] highlights that nanosystems formed from self-assembling dendrimers have great potential as novel and robust platforms for various biomedical applications. The supramolecular dendrimer nanosystem developed in this work can be further extended to radiotherapy, and to applications which combine radiotherapy and imaging,[4,5] for example, those using the radionuclide [^{177}Lu]Lu. We are working actively to realize these exciting possibilities.

We thank Michel Skandalovski (CERIMED, Aix-Marseille University) and Sandrine Pons (Faculty of Pharmacy, Aix-Marseille University) for technical support. This work was supported by the Ligue Nationale Contre le Cancer (LP, ZL), the ERA-Net EURONANOMED projects ''Target4Cancer'', ''NANOGLIO'' and ''TARBRAINFECT'' (LP), H2020 NMBP ''SAFE-N-MEDTECH'' (814607) (LP), China Scholarship Council (LD) and Italian Association for Cancer Research (IG17413) (SP). This article is based on work from COST Action CA 17140 ''Cancer Nanomedicine from the Bench to the Bedside'' supported by COST (European Cooperation in Science and Technology).

Conflicts of interest

There are no conflicts to declare.

Notes and references

1 M. L. James and S. S. Gambhir, *Physiol. Rev.*, 2012, **92**, 897–965.
2 D. Ni, E. B. Ehlerding and W. Cai, *Angew. Chem., Int. Ed.*, 2019, **58**, 2570–2579.
3 O. Israel, O. Pellet, L. Biassoni, D. De Palma, E. Estrada-Lobato, G. Gnanasegaran, T. Kuwert, C. la Fougère, G. Mariani, S. Massalha, D. Paez and F. Giammarile, *Eur. J. Nucl. Med. Mol. Imaging*, 2019, **46**, 1990–2012.
4 T. J. Wadas, E. H. Wong, G. R. Weisman and C. J. Anderson, *Chem. Rev.*, 2010, **110**, 2858–2902.
5 T. I. Kostelnik and C. Orvig, *Chem. Rev.*, 2019, **119**, 902–956.
6 H. Chen, W. Zhang, G. Zhu, J. Xie and X. Chen, *Nat. Rev. Mater.*, 2017, **2**, 17024.
7 C. Li, *Nat. Mater.*, 2014, **13**, 110.
8 E. K.-H. Chow and D. Ho, *Sci. Transl. Med.*, 2013, **5**, 216rv214.
9 H. Maeda, J. Wu, T. Sawa, Y. Matsumura and K. Hori, *J. Controlled Release*, 2000, **65**, 271–284.
10 E.-K. Lim, T. Kim, S. Paik, S. Haam, Y.-M. Huh and K. Lee, *Chem. Rev.*, 2015, **115**, 327–394.
11 P. Garrigue, J. Tang, L. Ding, A. Bouhlel, A. Tintaru, E. Laurini, Y. Huang, Z. Lyu, M. Zhang, S. Fernandez, L. Balasse, W. Lan, E. Mas, D. Marson, Y. Weng, X. Liu, S. Giorgio, J. Iovanna, S. Pricl, B. Guillet and L. Peng, *Proc. Natl. Acad. Sci. U. S. A.*, 2018, **115**, 11454–11459.
12 D. L. Bailey and K. P. Willowson, *Eur. J. Nucl. Med. Mol. Imaging*, 2014, **41**, 17–25.
13 E. W. Price and C. Orvig, *Chem. Soc. Rev.*, 2014, **43**, 260–290.
14 We were unable to obtain well-resolved NMR spectra for **In-2** because of the highly quadrupolar effect of the ^{115}In nucleus. For details, please see, *Handbook of High Resolution Multinuclear NMR*, ed. C. Brevard and P. Granger, John Wiley and Sons, Inc., 1981.
15 Z. Zhou, M. Cong, M. Li, A. Tintaru, J. Li, J. Yao, Y. Xia and L. Peng, *Chem. Commun.*, 2018, **54**, 5956–5959.
16 T. Wei, C. Chen, J. Liu, C. Liu, P. Posocco, X. Liu, Q. Cheng, S. Huo, Z. Liang, M. Fermeglia, S. Pricl, X.-J. Liang, P. Rocchi and L. Peng, *Proc. Natl. Acad. Sci. U. S. A.*, 2015, **112**, 2978–2983.
17 C. Chen, P. Posocco, X. Liu, Q. Cheng, E. Laurini, J. Zhou, C. Liu, Y. Wang, J. Tang, V. D. Col, T. Yu, S. Giorgio, M. Fermeglia, F. Qu, Z. Liang, J. J. Rossi, M. Liu, P. Rocchi, S. Pricl and L. Peng, *Small*, 2016, **12**, 3667–3676.
18 Y. Dong, T. Yu, L. Ding, E. Laurini, Y. Huang, M. Zhang, Y. Weng, S. Lin, P. Chen, D. Marson, Y. Jiang, S. Giorgio, S. Pricl, X. Liu, P. Rocchi and L. Peng, *J. Am. Chem. Soc.*, 2018, **140**, 16264–16274.

